Microelectronics Reliability 137 (2022) 114752

Contents lists available at ScienceDirect

Microelectronics Reliability

journal homepage: www.elsevier.com/locate/microrel

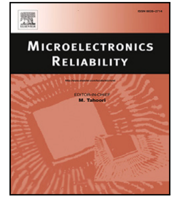

Influence of Interface Traps on MOSFET thermal coefficients and its effects on the ZTC current[☆]

R. García Cozzi [a], E. Redín [a], M. Garcia–Inza [a,b], L. Sambuco Salomone [a], A. Faigón [a,b], S. Carbonetto [a,b,*]

[a] Device Physics-Microelectronics Lab., INTECIN, Facultad de Ingeniería, Universidad de Buenos Aires, Av. Paseo Colón 850 (C1063ACV), Ciudad de Buenos Aires, Argentina

[b] The National Scientific and Technical Research Council of Argentina (CONICET), Ciudad de Buenos Aires, Argentina

ARTICLE INFO

Keywords:
MOS thermal coefficients
Interface traps
MOS sensors

ABSTRACT

Interface degradation-induced shifts of MOSFET thermal coefficients and zero temperature coefficient current (I_{ZTC}) were studied by monitoring the interface traps (N_{it}) growth in a thick oxide n-channel MOSFET due to exposure to ionizing radiation, and to further annealing at room temperature. A new physics-based compact model was proposed to account for the observed results, and to predict the evolution of these parameters as interface traps are generated during stress. Within a range (0–40°C) around room temperature, both the inverse of the mobility and the threshold voltage thermal coefficient varied roughly linear with N_{it}, with relative variations of 5.2×10^{-13} eV cm^2 and -9.33×10^{-13} eV cm^2, respectively. Furthermore, the dependence for I_{ZTC} with N_{it} can also be approximated to a linear expression, with a relative increment of 1.94×10^{-12} eV cm^2. The implications for temperature error mitigation in MOS sensors were discussed.

1. Introduction

Temperature changes affect the electrical characteristics of a metal–oxide–semiconductor field-effect transistor (MOSFET) due to its effects on both threshold voltage (V_T) and channel carriers mobility (μ). This issue is particularly relevant for sensor applications, such as ion-sensitive field-effect transistor (ISFET) [1–3] or MOS dosimeters [4–8], where the value of V_T is taken as a measure of the variable to be sensed, and the temperature-induced V_T-shift leads to misreadings. To mitigate this undesired effect, several error compensation techniques were proposed [9–14].

There is a device operation point at which V_T and μ temperature dependencies compensate each other, so this point remains unaffected by temperature variations [15]. The current at this bias point is known as the Zero Temperature Coefficient current (I_{ZTC}) and it is used for temperature error rejection in MOS sensors [16,17], but also in circuit design for analog/RF applications in a wide temperature range [18], and in current references for reading of the programmed states in multilevel phase change memories [19].

Interface traps growth along the device aging modify both V_T and μ temperatures dependencies, leading to a displacement of the ZTC point, which impoverishes temperature-error rejection [17,20]. As device dimensions shrink, this growth is accelerated by electrical stress even at low voltages becoming a major concern [21,22]. Regarding sensor applications, this effect is particularly relevant for MOS dosimeters as the exposure to ionizing radiation is known to increase interface traps generation [23].

In this work, a thick gate oxide MOSFET is exposed to ionizing radiation and traps are generated at the Si/SiO_2 interface. Before and after each irradiation session, and also during post-irradiation room temperature annealing, $I_D - V_{GS}$ curves are measured at different temperatures, and both interface traps density (N_{it}) and thermal parameters are obtained. From the analysis of the experimental results and based on previously well-established physical principles, a novel compact model is proposed to consider both temperature and interface traps effects simultaneously, leading to an expression for the change in the ZTC current with interface traps growth.

☆ This work was supported by Agencia Nacional de Promoción de la Investigación, el Desarrollo Tecnológico y la Innovación (ANPCyT) grant PICT-2014-1812, Universidad de Buenos Aires grants UBACyT 20020170100685BA and UBACyT 20020170200337BA.

* Corresponding author at: Device Physics-Microelectronics Lab., INTECIN, Facultad de Ingeniería, Universidad de Buenos Aires, Av. Paseo Colón 850 (C1063ACV), Ciudad de Buenos Aires, Argentina.

E-mail address: scarbonetto@fi.uba.ar (S. Carbonetto).

https://doi.org/10.1016/j.microrel.2022.114752
Received 21 February 2022; Received in revised form 10 August 2022; Accepted 16 August 2022
Available online 9 September 2022
0026-2714/© 2022 Elsevier Ltd. All rights reserved.

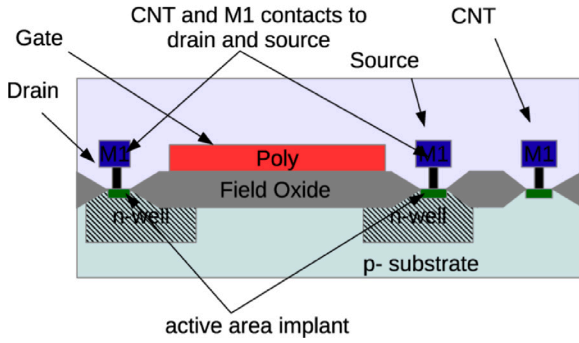

Fig. 1. Cross section of the device used in this paper [24].

2. Experiments and results

2.1. Device under test

The device under study is a thick oxide n-channel MOSFET fabricated in a standard CMOS process where the field oxide, which is normally used to isolate non-active areas of the chip, is used as gate oxide. The field oxide thickness in this fabrication process is t_{ox} = 566 nm. The device was fabricated to be used as a dosimeter and it was found useful to the present study given its high V_T sensitivity. A cross section of the device is presented in Fig. 1. The device was designed with geometry L = 25 µm and W = 110 µm and multiplicity M = 4, leading to an effective width $W_{eff} = M \times W$ = 440 µm. For more information on the device the reader can refer to [24,25].

2.2. Characteristic curves

To study the behavior of the thermal characteristic of the transistor, different sets of I_D vs V_{GS} curves with drain connected to gate ($V_{DS} = V_{GS}$) were measured. Each set or family represents a temperature sweep between 0 °C and 40 °C, with 10 °C steps with a precision temperature controller [26].

In order to investigate how the radiation affects the thermal parameters, the device was irradiated with a fixed gate bias V_{BIAS} = 12 V, while all other terminals were grounded. After irradiation, the family of curves were measured at different temperatures. After the last irradiation session, the device was stored at room temperature without any bias, and after some elapsed time a new set of curves was measured.

Fig. 2 shows the results for different accumulated radiation dose. After each irradiation, the family of curves shifts to lower voltages, due to increasing hole capture in the gate oxide. Conversely, in Fig. 3, where the family of curves are plotted for different elapsed times after irradiation, a voltage recovery occurs, with each set of curves shifting to higher voltages as time goes by. This recovery, also known as *fading*, is mainly driven by the slow thermal or tunneling neutralization or *annealing* of the radiation-induced oxide trapped charge, and can continue for days or even months after irradiation [27].

As mentioned in the introduction, another physical effect of radiation on MOS devices is the increase in interface traps density N_{it}. It is accepted that depassivation of interface traps is a two-stage process known as *Hole Trapping, Hydrogen Transport* [28]. When a hole is captured in an oxide trap, a Hydrogen ion (proton) is released and transported towards the Si–SiO_2 interface according to the local electric field. When the proton reaches the interface, it can react with a SiH bond (a passivated interface trap), forming a H_2 and leaving an unbonded Si behind (a dangling bond, or interface trap).

The only phenomena that is induced by radiation is the hole trapping process. Once the device is no longer exposed to radiation, protons may be still being transported within the oxide and can reach the interface several days after the irradiation is finished. This is why the

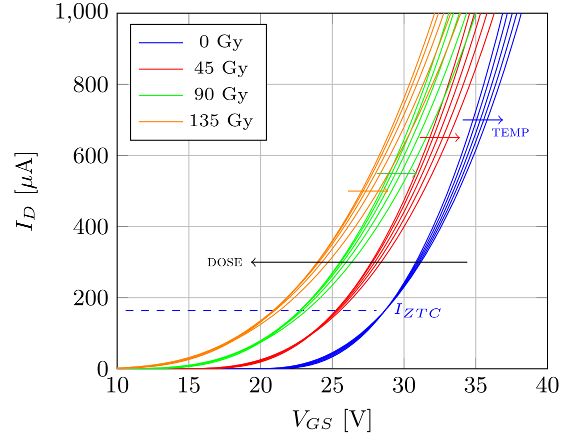

Fig. 2. Current–voltage family of curves for different accumulated radiation dose. Each family (each color group) consists of I_D vs. V_{GS} curves with drain connected to gate ($V_{DS} = V_{GS}$) at five different temperatures from 0 °C to 40 °C in 10 °C steps. The rightmost family (blue) is for the non-irradiated device. Colored arrows show the temperature increment for each family of curves.

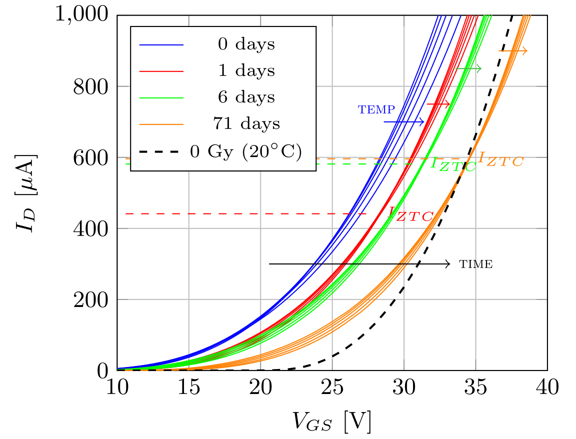

Fig. 3. Current–voltage family of curves at different elapsed times after completing a total dose of 180 Gy. Each family (each color group) consists of I_D vs. V_{GS} curves with drain connected to gate ($V_{DS} = V_{GS}$) at five different temperatures from 0 °C to 40 °C in 10 °C steps. The leftmost family (blue) was measured right after irradiation. Colored arrows show the temperature increment for each family of curves. The curve prior to any irradiation for 20 °C is show for reference (dashed black line).

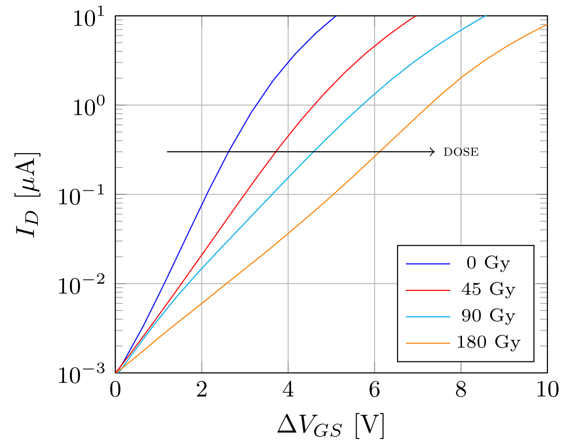

Fig. 4. Subthreshold region in semi-logarithmic scale for different accumulated dose. All curves correspond to the current–voltage characteristics in Fig. 2 at T = 20 °C, and the curves are shifted so that they coincide for current I_D = 1 nA, meaning that $\Delta V_{GS} = V_{GS} - V_{GS}(1\,\text{nA})$.

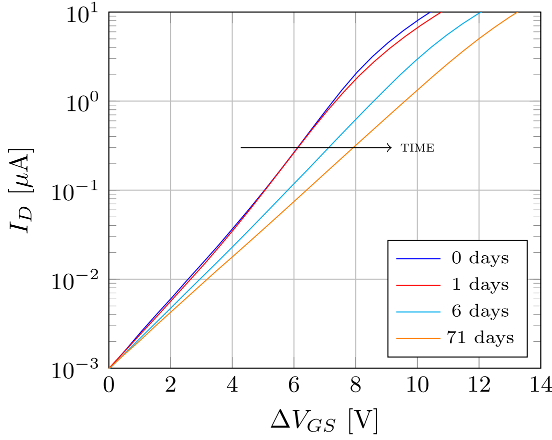

Fig. 5. Subthreshold region in semi-logarithmic scale for different periods of time after irradiation. All curves correspond to the current–voltage characteristics in Fig. 3 at T = 20 °C, and the curves are shifted so that they coincide for current I_D = 1 nA, meaning that $\Delta V_{GS} = V_{GS} - V_{GS}(1\,\text{nA})$. The decrease in the slope continues several days after irradiation is finished.

interface traps density increment can be observed even after radiation exposure ends.

The increase in N_{it} is directly related to the decrease in the MOS sub-threshold slope. The sub-threshold slope is the increment rate of the drain current with the gate voltage in a semi-logarithmic plot of the characteristic curves in the sub-threshold region. The consistent decrease in the sub-threshold slope shown in Figs. 4 and 5 means that interface trap density increases with absorbed dose and continues to increase days after irradiation is over.

3. Measurement analysis and modeling

To study how the MOSFET temperature coefficients change with radiation, the parameters k and V_T that model the drain current of the transistor in saturation regime, as shown in Eq. (1), were extracted for all the characteristic curves in both Fig. 2 and 3.

$$I_D = k\left(V_{GS} - V_T\right)^2 \tag{1}$$

where

$$k = \frac{\mu C_{ox}}{2}\frac{W}{L}; \tag{2}$$

C_{ox}, W and L are device constants. For a given device k is proportional to the inversion channel mobility (μ).

Likewise, sub-threshold slope values were extracted from the linear range in the characteristic semi-logarithmic curves at 20 °C for each of the measurements in Figs. 4 and 5. The change in the interface traps density was then calculated by means of [29]

$$\Delta N_{it} = \frac{C_{ox}}{q\, k_B\, T\, \ln(10)}\,\Delta S \tag{3}$$

where q is the elementary charge, k_B is the Boltzmann constant and ΔS, known as the *sub-threshold swing*, is the change in the inverse of the sub-threshold slope. ΔN_{it} is referred to the non-irradiated device $\Delta N_{it} = N_{it} - N_{it}(0\,\text{Gy})$.

A total of 40 sets of parameters were obtained, combining 5 different temperatures and 8 different interface traps density conditions. Four of these N_{it} conditions were estimated right after irradiation (Figs. 2 and 4), whereas the other four N_{it} conditions were estimated at different time elapsed after the last irradiation (Figs. 3 and 5).

As a summary of the results, Fig. 6 shows the change in the three estimated parameters at T = 20 °C with dose and with time after irradiation.

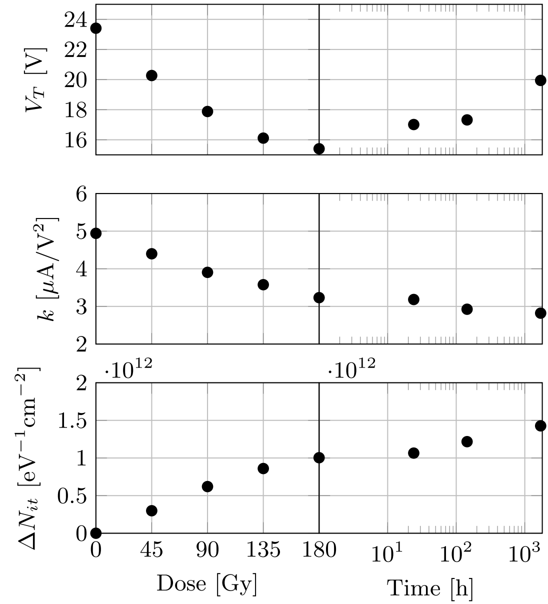

Fig. 6. Estimated parameters V_T, k (both at T = 20 °C) and ΔN_{it} and their evolution with accumulated dose and elapsed time since last irradiation.

3.1. Mobility temperature model

A mobility temperature model, derived from the one presented by Chain, et al. [30], is proposed to explain the experimental results. We start by simplifying Chain's model taking into account that:

(i) Coulombian scattering by bulk impurities can be neglected as it is relevant only at low temperatures;
(ii) in the small range of oxide fields where our measurements took place there is negligible dependence of the mobility on the electric field; and
(iii) bulk and source are short-circuited in our measurements.

Under these conditions, three sources of scattering remain:

(1) phonon scattering due to lattice vibration;
(2) surface roughness scattering due to the microscopic roughness of the Si–SiO_2 interface; and
(3) coulomb scattering from the Si–SiO_2 interface charges.

Therefore, Chain's mobility expression is reduced to:

$$\mu = \frac{\mu_0}{\left(1 + O_a\right)\left(\frac{T}{T_0}\right)^{3/2} + O_b\left(\frac{T}{T_0}\right)^{-1/2} + O_c\left(\frac{T}{T_0}\right)}. \tag{4}$$

μ_0 in (4) is the pre-irradiation value at T_0 = 20 °C and O_a, O_b, O_c are fitting parameters that account for phonon, roughness and interface charge scattering respectively, retaining the temperature dependence while absorbing the field dependence of Chain's equation in the new coefficients, according to considerations (i) to (iii) above.

The pre-irradiation experimental results were fitted with model (4). Assuming negligible the influence of interface charge due to an initial low interface traps density ($O_c \approx 0$), yields $O_a \approx -O_b \approx 0.5$ — exact values from regression are O_a = 0.493 ± 0.013 and O_b = −0.494 ± 0.012. With these values of O_a and O_b, and considering O_c = 0, the pre-irradiation mobility model can be reduced within our working temperature range, to — see Appendix:

$$\mu = \frac{\mu_0}{\left(\frac{T}{T_0}\right)^{5/2}} \tag{5}$$

the mobility temperature dependence empirically obtained in [31,32].

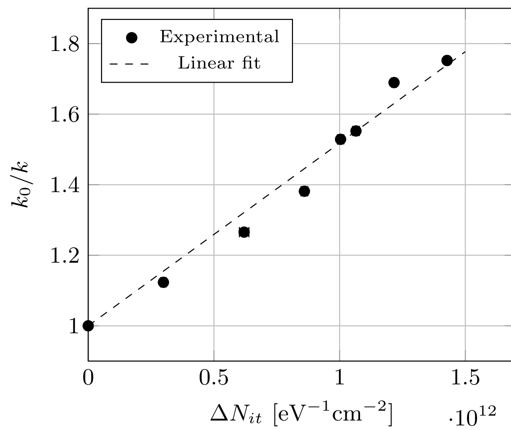

Fig. 7. Normalized values of parameter k vs. interface traps density. The α parameter is the slope of the linear fit (dashed line).

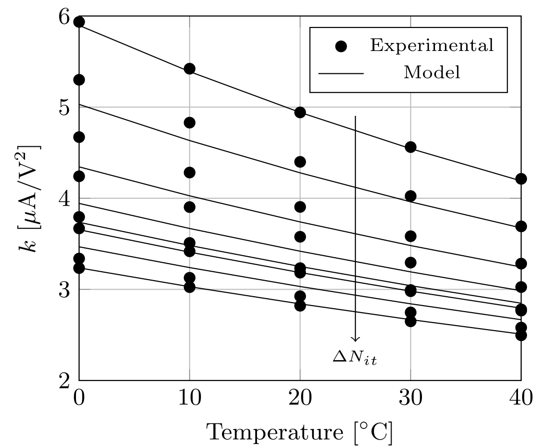

Fig. 8. Values of parameter k as a function of temperature and parameterized by interface traps density. Results estimated from measurements (markers) and corresponding simulation results from the model (lines) with $\alpha = 5.2 \times 10^{-13}$ eV cm^2 are shown. The arrow indicates the increment of interface traps between sets of values.

Concerning the mobility dependence with interface traps density N_{it}, the following empirical relationship:

$$\mu = \frac{\mu_0}{1 + \alpha \Delta N_{it}} \tag{6}$$

where μ_0 is the pre-irradiation value and α is a fitting parameter, was found by Sexton and Schwank [33].

Eq. (4) gives no information on how O_c changes with interface traps density creation, while equation (6) does not consider how temperature affects the mobility. Analyzing the results obtained for O_a and O_b and considering $T = T_0$, Eq. (4) is simplified to:

$$\mu = \frac{\mu_0}{1 + O_c}. \tag{7}$$

Comparing equation (7) with Eq. (6) we pose that the parameter O_c should be affected by interface traps creation, and hence propose that $O_c = \alpha\, \Delta N_{it}$ to account for this change, where α is the same parameter as in Eq. (6).

Finally, considering equation (4), the results obtained for parameters O_a and O_b, which lead to an equivalence with Eq. (5), and the proposed dependence of O_c with ΔN_{it}, the following model for the k parameter, proportional to the mobility, is obtained:

$$k = \frac{k_0}{\left(\frac{T}{T_0}\right)^{5/2} + \alpha\, \Delta N_{it} \left(\frac{T}{T_0}\right)}. \tag{8}$$

The parameter k_0 corresponds to k when the temperature is the reference temperature, $T = T_0 = 20$ °C in our case, and for the initial interface traps density, $\Delta N_{it} = 0$. For the device under test, $k_0 = 4.94\,\mu$A/V^2 which yields $\mu_0 = 92$ cm^2/(V s).

In Fig. 7, the inverse of the normalized k is plotted for $T = T_0 = 20$ °C. The linear fit of $k_0/k = 1 + \alpha\, \Delta N_{it}$ yield the value of $\alpha = (5.2 \pm 1.5) \times 10^{-13}$ eV cm^2, close to those obtained in other empirical studies [33,34]. With the measured k_0 and the α obtained from the linear fit, calculated curves in Eq. (8) are plotted along 40 experimental points (eight N_{it} times 5 temperature values) in Fig. 8 exhibiting a fairly good agreement.

3.2. Threshold voltage temperature coefficient

The MOSFET threshold voltage is given by

$$V_T = \Phi_{ms} + 2\Phi_B - \frac{1}{C_{ox}} \left(Q_{ox} + Q_{dep} + Q_{it}\right) \tag{9}$$

where Φ_{ms} is the metal–semiconductor work function difference, Φ_B is the bulk potential, and Q_{ox}, Q_{dep} and Q_{it} are the oxide, depletion and interface charge densities. Eq. (9) can be rewritten as:

$$V_T = V_{T_0} - \frac{1}{C_{ox}} Q_{ox} - \frac{1}{C_{ox}} Q_{it} \tag{10}$$

where V_{T_0} is the pre-irradiation threshold voltage. The temperature derivative of Eq. (10) yields the threshold voltage temperature coefficient θ_T:

$$\theta_T = \theta_{T_0} + \frac{1}{C_{ox}} \frac{\partial Q_{it}}{\partial T} \tag{11}$$

where θ_{T_0} is the pre-irradiation threshold voltage temperature coefficient and can be written as [15]:

$$\theta_{T_0} = \frac{\Phi_{ms}}{T} + 2\frac{\Phi_B}{T} + \frac{\sqrt{\epsilon_s q N_a}}{C_{ox}\sqrt{\Phi_B}} \frac{\partial \Phi_B}{\partial T}. \tag{12}$$

In Eq. (11) it is considered that the term for the oxide traps Q_{ox} is independent from the temperature variations. The interface charge density Q_{it} is given by [35]:

$$Q_{it} = -q \int_{E_v}^{E_c} N_{it}[E]\ f[E] dE \tag{13}$$

where $f[E]$ is the Fermi–Dirac distribution:

$$f[E] = \frac{1}{1 + e^{(E-E_F)/k_B T}}. \tag{14}$$

Taking into account that $E_F - E_v \gg k_B\, T$, the Fermi–Dirac distribution is approximately equal to 1 in almost all the energy range between E_v and E_F, even at the higher temperatures in our measurements. Thus, Eq. (13) can be written as:

$$Q_{it} \simeq -q\ N_{it}\ (E_F - E_v). \tag{15}$$

This N_{it} value is equal to the one obtained from the Sub-threshold Swing method, Eq. (3), and it represents the Interface Traps distribution mean value.

Finally, replacing (15) in (11), θ_T can be rewritten as:

$$\theta_T = \theta_{T_0} - \frac{q N_{it}}{C_{ox}} \frac{\partial (E_F - E_v)}{\partial T}. \tag{16}$$

In the studied temperature range, the relationship between $E_F - E_v$ and T is approximately linear, so the value of θ_T for each ΔN_{it} was calculated through the linear approximation of Eq. (16).

Fig. 9 shows the comparison between the calculated and experimental values of θ_T. The stronger *fading* effect present in the characteristic curves that were measured immediately after irradiation prevented the acquisition of reliable θ_T values, so these points were excluded from the figure. The progressive shift of the shown experimental values from the linear model could be explained by a residual presence of *fading* in the measurements.

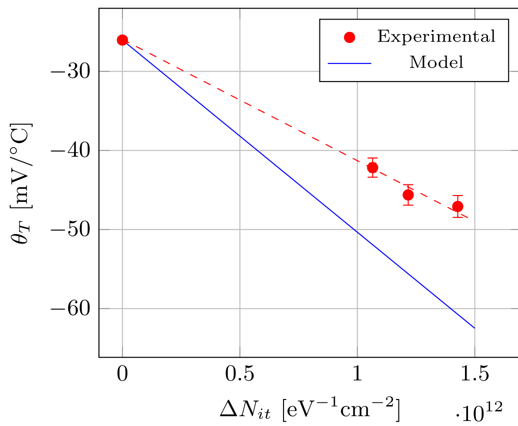

Fig. 9. Threshold voltage thermal coefficient vs. interface traps density. The red markers are the experimental results and the dashed red line is their linear fit. The blue line represents the model results. θ_{T_0} was evaluated from (12) using $N_a = 10^{17}$ cm^{-3}, $C_{ox} = 6.1$ nF/cm^2 and $\Phi_{ms} = -0.95$ V.

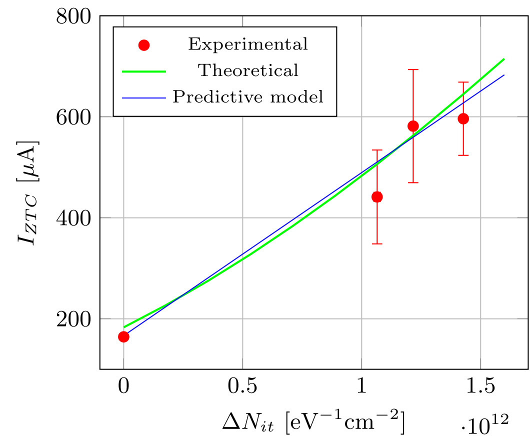

Fig. 10. I_{ZTC} current as a function of the in interface traps density ΔN_{it}: measured points (red markers) and theoretical model (blue markers).

The slope of the theoretical linear relationship between θ_T and ΔN_{it} yields

$$\frac{\theta_T}{\theta_{T_0}} = 1 + \gamma\, \Delta N_{it} \tag{17}$$

where $\gamma = -9.33 \times 10^{-13}$ eV cm^2.

3.3. Zero temperature coefficient current

One of the techniques to reduce the temperature error mentioned in Section 1 is to bias the sensor at the *Zero Temperature Coefficient Current* or ZTC current, defined as the drain current for which the temperature sensitivity of the MOS transistor is minimum. One problem associated with this method is that the ZTC current drifts with interface traps growth, so that with aging the device becomes more sensitive to temperature variation. In practice, this current is obtained by plotting the I_D vs V_{GS} characteristic of the transistor at different temperatures and finding the point at which all curves intersect, as shown in Fig. 3, a task that requires the use of a temperature controller and takes a considerable amount of time. In this section the variation of the ZTC current with absorbed dose will be studied and a model of its behavior will be presented.

When a MOSFET is biased at the ZTC point, the following condition holds [15,17,36]:

$$\frac{\partial I_D}{\partial T} = 0. \tag{18}$$

In Figs. 2 and 3 it can be seen that the ZTC current is found in the saturation regime. Remembering the drain current expression used in Section 3:

$$I_D = k\left(V_{GS} - V_T\right)^2. \tag{19}$$

Condition (18) can be applied to (19), which yields:

$$\frac{\partial k}{\partial T}(V_{GS} - V_T)^2 - 2k(V_{GS} - V_T)\theta_T = 0. \tag{20}$$

The solution to the previous quadratic equation is:

$$V_{GS} - V_T = \frac{2k\theta_T}{\frac{\partial k}{\partial T}}. \tag{21}$$

Replacing (21) in (19), the following expression of I_{ZTC} as a function of k, its temperature derivative, and θ_T can be obtained:

$$I_{ZTC} = 4k^3\left(\frac{\theta_T}{\frac{\partial k}{\partial T}}\right)^2. \tag{22}$$

From our obtained k model (8), its derivative was calculated:

$$\frac{\partial k}{\partial T} = \frac{-\frac{k_0}{T_0}\left(\frac{5}{2}\left(\frac{T}{T_0}\right)^{3/2} + \alpha\, \Delta N_{it}\right)}{\left(\left(\frac{T}{T_0}\right)^{5/2} + \alpha N_{it}\frac{T}{T_0}\right)^2}. \tag{23}$$

As with θ_T, the measured values of I_{ZTC} were also affected by residual fading. Taking this into account, the theoretical I_{ZTC} points for every corresponding ΔN_{it} were calculated using the θ_T model with the experimental slope in Fig. 9. The comparison of the experimental I_{ZTC} points and those calculated with expression (22) is shown in Fig. 10.

When the current–voltage (I–V) curves are closely examined near the ZTC condition, it can be seen that rather than a point, there is a bounded range of currents for which the temperature sensitivity is minimum. Therefore the experimental I_{ZTC} points were calculated as the mean intersection current for the different curves and the error as the standard deviation. It can be seen that the evolution of the experimental points with ΔN_{it} satisfies the theory in the measured range.

From Fig. 10, a linear model is proposed to predict the I_{ZTC} value to be used as reference current in a radiation measurement:

$$\frac{I_{ZTC}}{I_{ZTC_0}} = 1 + \beta\, \Delta N_{it} \tag{24}$$

where $\beta = 1.94 \times 10^{-12}$ eV cm^2.

Eq. (24) requires only the N_{it} variation, which is obtained through the sub-threshold slope, to predict the new I_{ZTC} value.

4. Discussion

A thick gate oxide MOSFET was stressed by radiation exposure in order to register the change in its thermal parameters. From the measurements of the characteristic curves of the transistor, the electric parameter V_T and k (proportional to the mobility) were obtained at different temperatures, and also the interface traps density was estimated, recording their change with the absorbed dose and also with the time after irradiation. Fig. 6 summarizes the shift in these parameters for $T = 20$ °C. For V_T, radiation causes a shift towards lower values due to holes being captured in oxide traps. The interface traps generation (ΔN_{it}) also affects the change in V_T but in the different direction than the oxide traps. This means that while the device is irradiated, the hole trapping process rules the change in V_T. Once the irradiation is finished, the hole trapping process ceases, and the observed recovery of V_T is due to both the interface traps contribution which continues and partial neutralization of the oxide trapped charge that may occur. This is a well known behavior for n-channel devices [37,38]. The

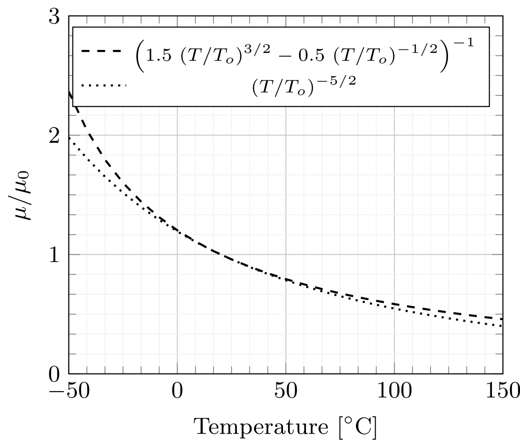

Fig. 11. Comparison between both models for mobility dependence with temperature.

mobility (proportional to the parameter k) decreases with the radiation exposure, and continues to decrease after the stress, showing no recovery. This is the expected behavior as the change in mobility is related with the increase of interface traps density, which continues to grow after irradiation [28]. This behavior with irradiation has been already observed [27,28,39,40], and a similar behavior can be observed also with other stress mechanisms such as Negative Bias Temperature Instability [41].

Before addressing the experimental results on the thermal parameters, we would like to make some remarks about expression (8) obtained in this work relating mobility (or k parameter of the transistor) with temperature and interface traps density. The expression is based on the theoretical expression (4) a simplified version of Chain's [30] which was found to be equal at first order in temperature (see Appendix) with the semi-empirical expressions found in [31,32] in case surface contribution is disregarded, $O_c = 0$, and $O_a \approx -O_b \approx 0.5$ in (4) as surprisingly was found through our measurements. The surface contribution was built combining the empirical dependence of mobility with interface traps density at fixed temperature found by Sexton and Schwank [33], with the theoretical temperature dependence of the interface charge scattering on the mobility through the parameter O_c in expression (4) [30], completing the unified expression (8) giving the dependence $k = k(T, \Delta N_{it})$.

From the experimental results we obtained $O_a \approx -O_b \approx 0.5$ in (4), $\alpha = (5.2\pm1.5)\times10^{-13}$ eV cm^2 in Eq. (8), the coefficient of ΔN_{it} in (17) was calculated to be $\gamma = -9.33\times10^{-13}$ eV cm^2, and $I_{ZTC_0} = 160.7$ µA and $\beta = 1.94\times10^{-12}$ eV cm^2 in (24). The I_{ZTC_0} is a completely sample dependent parameter, but the other ones can be compared with references in the literature and deserve some discussion.

The result $O_a \approx -O_b \approx 0.5$ in (4) is after our demonstration of its equivalence with (5), consistent with all those works where expression (5) fits experimental results [31,32]. Even though this result may seem specific of our investigation and the fitting parameters obtained in this work, the fact that several workgroups agree that the semi-empirical expression (5) is valid, suggests that this agreement is of a general matter. Fig. 11 shows both Chain's model for mobility variation with temperature and the semi-empirical model within an extended temperature range. It can be seen that their agreement is almost perfect within the experimental temperature range, but also the error between both models is less than 10% in the range between −35 °C and 135 °C. Returning to Chain's expression, according to the results of the present work, it could be enriched giving U_{c1} a linear dependence with ΔN_{it}.

As can be seen the only fitting parameter in our expression (8) is α (k_0 is measured on non-irradiated devices). It was obtained from fitting the family of curves in Fig. 8 to be $\alpha = (5.2 \pm 1.5) \times 10^{-13}$ eV cm^2 which compares well with values found in the literature as seen in Table 1 despite being a process dependent parameter [34].

Table 1
Comparison of the obtained fitting parameter α with other ones found in the literature.

Article	α [$\times10^{-13}$ eV cm^2]
This paper	5.2 ± 1.5
Sexton, et al. [33]	7.0 ± 1.3
Galloway, et al. [34]	8 ± 2

Even considering the misfits observed in Fig. 8 between experimental and modeled points the entire picture shows a rather good agreement. The experimental points entail some uncertainties due mainly to the fact that the experimental procedure required temperature changes and stabilization time within which the device may have been affected by two phenomena:

(i) the annealing of trapped charge (fading) [40] and
(ii) the creation of interface traps [39,40].

Both phenomena would recover V_T and shift the different IV curves to higher voltage, and may also stretch-out the curves in the sub-threshold region. Given the short time elapsed during the IV measurement, we consider that the instability occurred mainly between measurements. Both phenomena are correlated [39], and decrease with the elapsed time from irradiation. As days go by, the time needed for the experimental procedure becomes relatively negligible, and so does the instability. For this reason we give more weight in the fitting to those points with longer post irradiation elapsed time. This was explicitly done in Figs. 9 and 10 where only those points were taken into account, and even these remaining points are considered to be affected by the same effect causing the deviation of the experimental points from the model line in Fig. 9 which is thus a theoretical limit to the experimental results.

The presented results are particularly relevant for MOS dosimeters as interface traps creation occurs along the radiation exposure. The methods employed to minimize temperature-induced error, either by biasing the sensor at I_{ZTC} or by applying a correction that depends on temperature changes are, therefore, not reliable unless a periodic update of the thermal parameters is performed [8,17,20]. The model presented here simplifies this task.

5. Conclusions

The thermal characteristics of MOSFETs and the effects of interface traps growth on the thermal parameters were studied. A physics based model for the variation of the I_{ZTC} with the interface traps buildup was developed. In this model the temperature effects on mobility, as well as the effects of interface traps on both mobility and Threshold Voltage Temperature Coefficient were combined in order to be able to predict how the I_{ZTC} would change in response to the creation of interface traps. In the range studied around room temperature, it was observed that the dependency of I_{ZTC} with ΔN_{it} is very close to its linear regression, hence a simplified empirical linear relationship was proposed, which showed fair agreement with experimental data.

CRediT authorship contribution statement

R. García Cozzi: Conceptualization, Methodology, Formal analysis, Writing – original draft, Visualization. **E. Redín:** Investigation, Supervision, Resources. **M. Garcia–Inza:** Investigation, Supervision, Funding acquisition, Resources. **L. Sambuco Salomone:** Conceptualization, Methodology, Investigation. **A. Faigón:** Conceptualization, Methodology, Investigation, Supervision, Funding acquisition. **S. Carbonetto:** Conceptualization, Methodology, Investigation, Writing – review & editing, Visualization, Supervision, Formal analysis.

Declaration of competing interest

The authors declare that they have no known competing financial interests or personal relationships that could have appeared to influence the work reported in this paper.

Data availability

Data will be made available on request.

Appendix. Mobility expression reduction

We begin replacing equation (4) with the parameters obtained by fitting the pre-irradiation experimental results:

$$\mu = \frac{\mu_0}{1.5\left(\frac{T}{T_0}\right)^{3/2} - 0.5\left(\frac{T}{T_0}\right)^{-1/2}} \tag{25}$$

where O_c in (4) was taken to be 0 on the non-irradiated sample.

Given that in other studies a different mobility temperature dependence was found – proportional to $T^{-5/2}$ – the relationship between both representations for the obtained parameter values was explored, finding that they have identical first order polynomial approximation:

$$\left(\frac{T}{T_0}\right)^{3/2} = \left(1+\frac{\Delta T}{T_0}\right)^{3/2} \simeq 1+\frac{3}{2}\left(\frac{\Delta T}{T_0}\right)$$
$$\left(\frac{T}{T_0}\right)^{-1/2} = \left(1+\frac{\Delta T}{T_0}\right)^{-1/2} \simeq 1-\frac{1}{2}\left(\frac{\Delta T}{T_0}\right)$$
$$\left(\frac{T}{T_0}\right)^{5/2} = \left(1+\frac{\Delta T}{T_0}\right)^{5/2} \simeq 1+\frac{5}{2}\left(\frac{\Delta T}{T_0}\right)$$

Therefore

$$1.5\left(\frac{T}{T_0}\right)^{3/2} - 0.5\left(\frac{T}{T_0}\right)^{-1/2} \simeq$$
$$1.5\left[1+\frac{3}{2}\left(\frac{\Delta T}{T_0}\right)\right] - 0.5\left[1-\frac{1}{2}\left(\frac{\Delta T}{T_0}\right)\right] =$$
$$1+\frac{5}{2}\left(\frac{\Delta T}{T_0}\right) \simeq \left(\frac{T}{T_0}\right)^{5/2}$$

The above result allows the following approximation in the working temperature range, in which $\Delta T/T_0 = 20/298 \simeq 0.067$:

$$1.5\left(\frac{T}{T_0}\right)^{3/2} - 0.5\left(\frac{T}{T_0}\right)^{-1/2} \simeq \left(\frac{T}{T_0}\right)^{5/2} \tag{26}$$

Eq. (25) can then be simplified to (5).

References

[1] K. Nakazato, An integrated ISFET sensor array, Sensors 9 (11) (2009) 8831–8851.
[2] C. Jimenez-Jorquera, J. Orozco, A. Baldi, ISFET based microsensors for environmental monitoring, Sensors 10 (1) (2009) 61–83.
[3] N. Moser, J. Rodriguez-Manzano, T.S. Lande, P. Georgiou, A scalable ISFET sensing and memory array with sensor auto-calibration for on-chip real-time DNA detection, IEEE Trans. Biomed. Circuits Syst. 12 (2) (2018) 390–401.
[4] L. Adams, A. Holmes-Siedle, The development of a MOS dosimetry unit for use in space, IEEE Trans. Nucl. Sci. 25 (6) (1978) 1607–1612.
[5] M.J. Butson, A. Rozenfeld, J.N. Mathur, M. Carolan, T.P. Wong, P.E. Metcalfe, A new radiotherapy surface dose detector: The MOSFET, Med. Phys. 23 (5) (1996) 655–658.
[6] A.B. Rosenfeld, MOSFET dosimetry on modern radiation oncology modalities, Radiat. Prot. Dosim. 101 (1–4) (2002) 393—398.
[7] I.S. Kwan, A.B. Rosenfeld, Z. Qi, D. Wilkinson, M. Lerch, D.L. Cutajar, M. Safavi-Naeni, M. Butson, J.A. Bucci, Y. Chin, V.L. Perevertaylo, Skin dosimetry with new MOSFET detectors, Radiat. Meas. 43 (2008) 929–932.
[8] M. Garcia-Inza, M. Cassani, S. Carbonetto, M. Casal, E. Redín, A. Faigón, 6 MV LINAC characterization of a MOSFET dosimeter fabricated in a CMOS process, Elsevier Radiat. Measur. 117 (2018) 63–69.
[9] Wen-Yaw Chung, Yeong-Tsair Lin, D.G. Pijanowska, Chung-Huang Yang, Ming-Chia Wang, A. Krzyskow, W. Torbicz, New ISFET interface circuit design with temperature compensation, Microelectron. J. 37 (2006) 1105–1114.
[10] E. Garcia-Moreno, E. Isern, M. Roca, R. Picos, J. Font, J. Cesari, A. Pineda, Temperature compensated floating gate MOS radiation sensor with current output, IEEE Trans. on Nucl. Sci. 60 (5) (2013) 4026–4030.
[11] M. Garcia-Inza, S.H. Carbonetto, J. Lipovetzky, A. Faigon, Radiation sensor based on MOSFETs mismatch amplification for radiotherapy applications, IEEE Trans. Nucl. Sci. 63 (3) (2016) 1784–1789.
[12] M.A. Carvajal, M.S. Martínez-García, D. Guirado, A. Martínez-Olmos, A.J. Palma, Thermal compensation technique using the parasitic diode for DMOS transistors, Sensors Actuators 249 (2016) 249–255.
[13] R. Bhardwaj, S. Sinha, N. Sahu, S. Majumder, P. Narang, R. Mukhiya, Modeling and simulation of temperature drift for ISFET-based pH sensor and its compensation through machine learning techniques, Int. J. Circ. Theor. Appl. 47 (2019) 954–970.
[14] S. Carbonetto, M. Echarri, J. Lipovetzky, M. Garcia-Inza, A. Faigón, Temperature-compensated MOS dosimeter fully integrated in a high-voltage 0.35μm CMOS process, IEEE Trans. Nucl. Sci. 67 (6) (2020) 1118–1124.
[15] I.M. Filanovsky, A. Allam, Mutual compensation of mobility and threshold voltage temperature effects with applications in CMOS circuits, IEEE Trans. Circ. Syst. – I 48 (7) (2001) 876–884.
[16] P.K. Chan, D.Y. Chen, A CMOS ISFET interface circuit with dynamic current temperature compensation technique, IEEE Trans. Circ. Syst. – I 54 (1) (2007) 119–129.
[17] S.H. Carbonetto, M.A. García-Inza, J. Lipovetzky, E.G. Redin, L. Sambuco Salomone, A. Faigón, Zero temperature coefficient bias in MOS devices, dependence on interface traps density, application to MOS dosimetry, IEEE Trans. Nucl. Sci. 58 (6) (2011) 3348–3353.
[18] P.K. Sahu, S.K. Mohapatra, K.P. Pradhan, Zero temperature-coefficient bias point over wide range of temperatures for single- and double-gate UTB-SOI n-MOSFETs with trapped charges, Mater. Sci. Semicond. Process. 31 (2015) 175–183.
[19] A. Cabrini, F. Gallazzi, G. Torelli, Current reference scheme for multilevel phase-change memory sensing, in: Proceedings of the European Conference on Solid-State Circuits, ESSCIRC 2011, 2011, pp. 419–422.
[20] M.S. Martínez-García, A.J. Palma, M. Lallena-Arquillo, A. Jaksic, J. Torres del Río, D. Guirado Llorente, J. Banqueri, M.A. Carvajal, Accuracy improvement of MOSFET dosimeters in case of variation in thermal parameters, IEEE Trans. Nucl. Sci. 62 (2) (2015) 487–493.
[21] T. Grasser, B. Kaczer, B. O'Sullivan, G. Rzepa, B. Stampfer, M. Waltl, The mysterious bipolar bias temperature stress from the perspective of gate-sided hydrogen release, in: 2020 IEEE International Reliability Physics Symposium, IRPS, 2020, pp. 1–6.
[22] S. Kumar, R. Anandkrishnan, N. Parihar, S. Mahapatra, A stochastic framework for the time kinetics of interface and bulk oxide traps for BTI, SILC and TDDB in MOSFETs, IEEE Trans. Electron Dev. 67 (11) (2020) 4741–4748.
[23] D.M. Fleetwood, Evolution of total ionizing dose effects in MOS devices with Moore's law scaling, IEEE Trans. Nucl. Sci. 65 (8) (2018) 1465–1481.
[24] J. Lipovetzky, M. Garcia-Inza, S. Carbonetto, M.J. Carra, E.G. Redin, L.S. Salomone, A. Faigon, Field oxide n-channel MOS dosimeters fabricated in CMOS processes, IEEE Trans. Nucl. Sci. 60 (6) (2013) 4683–4691.
[25] M. Garcia-Inza, S. Carbonetto, J. Lipovetzky, M.J. Carra, L. Sambuco Salomone, E.G. Redin, A. Faigon, Switched bias differential MOSFET dosimeter, IEEE Trans. Nucl. Sci. 61 (3) (2014) 1407–1413.
[26] R.G. Cozzi, S. Carbonetto, A. Faigon, Peltier based temperature controller for MOS dosimeter characterization, in: 2019 Argentine Conference on Electronics, CAE, Mar Del Plata, Argentina, 2019, pp. 82–85.
[27] P.J. McWhorter, S.L. Miller, W.M. Miller, Modeling the anneal of radiation-induced trapped holes in a varying thermal environment, IEEE Trans. Nucl. Sci. 37 (6) (1990) 1682–1689.
[28] F.B. McLean, A framework for understanding radiation-induced interface states in SiO_2 MOS structures, IEEE Trans. Nucl. Sci. 27 (6) (1980) 1651–1657.
[29] T.P. Ma, P.V. Dressendorfer, Ionizing Radiation Effects in MOS Devices and Circuits, John Willey & Sons, 1989.
[30] K. Chain, Jian-hui. Huang, J. Duster, P.K. Ko, C. Hu, A MOSFET electron mobility model of wide temperature range (77–400 K) for IC simulation, Semicond. Sci. Technol. 12 (1997) 355–358.
[31] S.A. Schwarz, S.E. Russek, Semi-empirical equations for electron velocity in silicon: Part II-MOS inversion layer, IEEE Trans. Elec. Dev. 30 (12) (1983) 1634–1639.
[32] G. Baccarani, A.M. Mazzone, C. Morandi, The diffuse scattering model of effective mobility in the strongly inverted layer of MOS transistors, Solid-State Electron. 17 (1974) 785–789.
[33] F.W. Sexton, J.R. Schwank, Correlation of radiation effects in transistors and integrated circuits, IEEE Trans. Nucl. Sci. 32 (6) (1985) 3975–3981.
[34] K.F. Galloway, M. Gaitan, T.J. Russell, A simple model for separating interface and oxide charge effects in MOS device characteristics, IEEE Trans. Nucl. Sci. 31 (6) (1984) 1497–1501.
[35] S.M. Sze, Physics of Semiconductor Devices, third ed., John Wiley & Sons, Inc., 2006.

[36] G. Sarrabayrouse, S. Siskos, Radiation dose measurment using MOSFETs, IEEE Instrum. Measur. Mag. 1 (2) (1998) 26–34.

[37] P.S. Winokur, J.R. Schwank, P.J. McWorther, Correlating the radiation response of MOS capacitors and transistors, IEEE Trans. Nucl. Sci. 31 (6) (1984) 1453–1460.

[38] P.J. McWhorter, P.S. Winokur, Simple technique for separating the effects of interface traps and trapped-oxide charge in metal–oxide–semlconductor transistors, Appl. Phys. Lett. 48 (1986) 133–135.

[39] M.R. Shaneyfelt, J.R. Schwank, D.M. Fleetwood, P.S. Winokur, Effects of irradiation temperature on MOS radiation response, IEEE Trans. Nucl. Sci. 45 (3) (1998) 1372–1378.

[40] S.M. Djoric-Veljkovic, I.D. Manic, V.S. Davidovic, D.M. Dankovic, S.M. Golubovic, N.D. Stojadinovic, Annealing of radiation-induced defects in burn-in stressed power VDMOSFETs, Nucl. Technol. Radiat. Prot. 26 (1) (2011) 18–24.

[41] N. Stojadinovic, D. Dankovic, I. Manic, V. Davidovic, S. Djoric-Veljkovic, S. Golubovic, Impact of negative bias temperature instabilities on lifetime in p-channel power VDMOSFETs, in: 8th International Conference on Telecommunications in Modern Satellite, Cable and Broadcasting Services, 2007.